



UNIVERSITY OF LEEDS

This is a repository copy of *Thermal boundary layer structure in convection with and without rotation*.

White Rose Research Online URL for this paper:
<http://eprints.whiterose.ac.uk/168188/>

Version: Published Version

Article:

Long, RS orcid.org/0000-0001-9891-6233, Mound, JE orcid.org/0000-0002-1243-6915, Davies, CJ orcid.org/0000-0002-1074-3815 et al. (1 more author) (2020) Thermal boundary layer structure in convection with and without rotation. *Physical Review Fluids*, 5 (11). 113502. ISSN 2469-990X

<https://doi.org/10.1103/physrevfluids.5.113502>

©2020 American Physical Society. Uploaded in accordance with the publisher's self-archiving policy.

Reuse

Items deposited in White Rose Research Online are protected by copyright, with all rights reserved unless indicated otherwise. They may be downloaded and/or printed for private study, or other acts as permitted by national copyright laws. The publisher or other rights holders may allow further reproduction and re-use of the full text version. This is indicated by the licence information on the White Rose Research Online record for the item.


Takedown

If you consider content in White Rose Research Online to be in breach of UK law, please notify us by emailing eprints@whiterose.ac.uk including the URL of the record and the reason for the withdrawal request.





eprints@whiterose.ac.uk
<https://eprints.whiterose.ac.uk/>

Thermal boundary layer structure in convection with and without rotation

Robert S. Long ^{*}

EPSRC Centre for Doctoral Training in Fluid Dynamics, University of Leeds, Leeds LS2 9JT, United Kingdom

Jon E. Mound  and Christopher J. Davies 

School of Earth and Environment, University of Leeds, Leeds LS2 9JT, United Kingdom

Steven M. Tobias 

Department of Applied Mathematics, University of Leeds, Leeds LS2 9JT, United Kingdom



(Received 7 May 2020; accepted 18 September 2020; published 6 November 2020)

Convection occurs in many settings from metal production to planetary interiors and atmospheres. To understand the dynamics of these systems it is vital to be able to predict the heat transport which is controlled by the thermal boundary layers (TBL). An important issue in the study of convective fluid dynamics is then to determine the temperature distribution within these thin layers in the vicinity of the bounding walls. Deviations from the classical Rayleigh-Bénard convection paradigm such as the addition of rotation or fixed heat-flux (rather than fixed temperature) boundaries compromise the standard ways of defining the width of the TBL. We propose an alternative method for defining the TBL using the location at which the advective and conductive contributions to the heat transport become equal. We show that this method can be robustly applied to two-dimensional (2D) nonrotating convection between no-slip boundaries with fixed temperature or fixed heat-flux thermal boundary conditions and three-dimensional (3D) rotating convection simulations with free-slip boundaries.

DOI: [10.1103/PhysRevFluids.5.113502](https://doi.org/10.1103/PhysRevFluids.5.113502)

I. INTRODUCTION

Thermally driven flows are important in many industrial and natural settings including metal production [1], planetary atmospheres [2], solar and stellar bodies [3], and Earth's liquid metal outer core [4]. In astro- and geophysical settings rotation is an important factor in determining the flow dynamics. Turbulent rotating convection is responsible for internally generated magnetic fields [5] and the emitted heat-flux patterns of planets and stars [2]. However, the convective state of these systems cannot be reproduced by numerical or physical experiments owing to the vast range of spatial and temporal scales that need to be resolved. It is common practice to study the idealized system of Rayleigh-Bénard convection (RBC) but to understand real systems we must incorporate the effects of rotation and different boundary conditions.

Historically, the dynamics of RBC has been characterized by the heat transfer owing to the ease of using temperature sensors in laboratory experiments [6–8]. The majority of studies assume global heat transport dynamics implicitly describe the bulk dynamics, however, more recent studies conclude that the convective heat transport is determined by the boundary layer dynamics [9–11]. The theoretical framework of Grossmann and Lohse [12] describes the heat transport in RBC over a large range of parameter space by explicitly separating the dissipation contributions from the

*scr1@leeds.ac.uk

boundary layer and fluid bulk [12–14]. In rotating RBC two regimes of heat transport exist—one being rotationally constrained and one weakly rotating which resembles RBC. This transition is thought to be described by the dynamics of the thermal boundary layer; two key arguments include that of King *et al.* [9], who suggested that the transition to the weakly rotating regime occurs when the thermal boundary layer becomes thinner than the mechanical boundary layer [9], and Julien *et al.* [11], who proposed that the transition occurs when the thermal boundary layer loses geostrophic balance [15]. To elucidate the physics of flow transitions in thermal convection it would be useful to have a robust definition of the thermal boundary layer that can be broadly applied to different configurations.

We consider RBC with and without rotation. The RBC paradigm [16,17] consists of a plane layer of incompressible fluid (of depth h) constrained between two rigid horizontal boundaries. The fluid is gravitationally destabilized by a constant temperature difference, ΔT , between the boundaries. For a fixed aspect ratio, the nondimensional parameters governing the nonrotating system are the Rayleigh number, Ra , characterizing the importance of buoyancy forcing to resistive effects, and the Prandtl number, Pr , the ratio of the viscous and thermal diffusivities, given respectively as

$$Ra = \frac{\alpha g \Delta T h^3}{\nu \kappa}, \quad Pr = \frac{\nu}{\kappa}. \quad (1)$$

Here α denotes the thermal expansion coefficient, g the gravitational acceleration, ν the kinematic viscosity, and κ the thermal diffusivity. Convective fluid motions transport heat across the fluid layer and their efficiency is quantified by the Nusselt number, Nu , defined as the ratio of total heat transport to that of the conductive flux in the flow. The Nusselt number is defined as

$$Nu = \frac{qh}{k\Delta T}, \quad (2)$$

where q is the heat-flux and k is the fluid's thermal conductivity.

In the absence of rotation, turbulent convection mixes the fluid bulk and the temperature within the interior becomes more isothermal as Ra is increased. For Boussinesq convection the entire temperature drop across the fluid layer is then accommodated by the symmetric thermal boundary layers (TBLs). In this idealized case, the amount of heat transported across the layer can be related to the thickness of the TBL, δ . Within the TBL, heat transport is purely conductive and so we expect [18,19]

$$\frac{\delta}{h} = \frac{1}{2Nu}. \quad (3)$$

The thermal boundary layers are laminar (and conductive) over the range of Ra investigated in this study.

An important issue in the study of convective fluid dynamics is then to determine the thickness of the TBL and the corresponding temperature distribution within the TBL. Estimates of the TBL originally started in nonrotating convection experiments using fluids of moderate Pr . Two methods have been widely used to define δ relying on either the temporally and horizontally averaged temperature profile, ϑ , or on the root-mean-square temperature fluctuation, σ . In the first method, which we refer to as “linear intersection”, the extrapolation of the linear portion of ϑ near the boundary to the isothermal value defines δ [20–23]. The second method, termed “local maxima”, defines δ by the location of the local maxima in the σ profile [24–26]. An example of both methods can be seen in Fig. 1(a), which shows the TBL of a numerical solution.

Laboratory experiments of RBC typically drive convection by prescribing a fixed temperature on the boundaries rather than a fixed heat-flux [27–29]. Thermal boundary conditions have significant effects near convective onset, with fixed heat-flux conditions decreasing the critical Rayleigh number and increasing the preferred wavelength [30]. The longer wavelength of fixed heat-flux convection may also be important in determining convective patterns in the fully nonlinear regime [31]. In the turbulent regime Johnston and Doering [32] showed that over the range

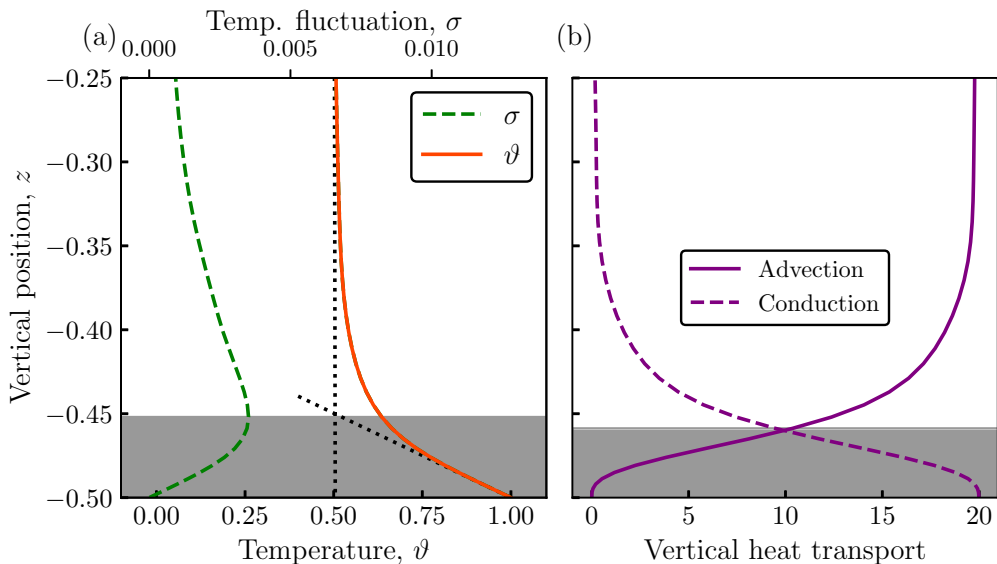


FIG. 1. Results from the model with $Ra = 3 \times 10^6$ and fixed temperature boundaries. Only the lowest quarter of the domain is shown to focus on behavior near the boundary. (a) Vertical profiles of temperature (solid orange) and rms fluctuation (dashed green). The dotted black lines show linear fits to ϑ at middepth and close to the boundaries. The gray shaded region shows the thermal boundary layer defined by the maxima in the σ profile. (b) Vertical profiles of advective (solid purple) and conductive (dashed purple) heat transport. The gray shaded regions show the intersection of the heat transport contributions.

$10^6 \leq Ra \leq 10^{10}$ the time averaged temperature profiles and values of Nu are indistinguishable between fixed temperature and fixed heat-flux conditions. If the Nu values are the same between both cases then we should expect δ to also be indistinguishable. Over a similar range of Ra the experimental study of Verzicco and Sreenivasan [33] found that, although the temperature profiles were indistinguishable between the different thermal boundary conditions, the profiles of σ behaved very differently. Applying the local maxima method to a fixed heat-flux boundary, Verzicco and Sreenivasan [33] found that the peak was always on the boundary, predicting $\delta = 0$; they instead chose to treat this boundary using the linear intersection method. We will address this discrepancy in Sec. III, where we introduce a method based on the vertical heat transport. This definition is shown in Fig. 1(b).

In contrast with the RBC paradigm, astro- and geophysical flows are heavily influenced by the effects of rotation [34,35]. For the simplest model of rotating RBC, the fluid layer is rotated about the vertical with constant angular frequency, Ω . A third dimensionless parameter, the Ekman number, E , measures the relative importance of viscosity to rotation,

$$E = \frac{\nu}{2\Omega h^2}. \quad (4)$$

Different regimes of rotating convection exist based on the relative importance of rotation and buoyancy forces [9,36–38]. For a given E , below some transitional value of Ra there is rotationally constrained convection, and above this there is weakly rotating convection. Rotationally constrained flows have a tendency to form columnar flow structures aligned with the rotation axis [39,40]. These columnar structures are able to sustain interior temperature gradients over many orders of Ra [41]. For a fixed value of Ra the size of the interior temperature gradients increases with decreasing E [26] and within this regime δ is poorly described by Eq. (3). The weakly rotating regime resembles nonrotating convection having an isothermal fluid bulk and boundary layers described

by Eq. (3) [26]. The standard definitions of the TBL have not been systematically tested in rotating RBC and in Sec. III we report the outcome of this investigation.

We present a systematic numerical investigation of convection with and without rotation to examine the robustness of existing methods for defining the TBL thickness. We use simulations of RBC with two different thermal boundary conditions, fixed temperature and fixed heat-flux, and a suite of rotating simulations with fixed temperature boundaries. The limitations of the local maxima and linear intersection methods leads us to suggest an alternative approach based on the vertical heat transport. In Sec. II we outline the numerical implementation with which our solutions are computed and the different methods used to define the TBL. In Sec. III we assess the robustness of these different methods in the different regimes of rotating convection. Finally, an extended discussion is provided in Sec. IV.

II. METHODS

A. Governing equations

We use numerical simulations of horizontally periodic RBC with and without rotation to test the robustness of each method for defining the TBL. The nondimensional velocity, \mathbf{u} , and temperature, T , are evolved by computing the numerical solutions of the Navier-Stokes and temperature equations in dimensionless form.

1. Nonrotating RBC

We investigate the effect of different thermal boundary conditions on each of the methods to define the TBL by performing a suite of two-dimensional RBC simulations. Our configuration is the same as that of [32]. We use a domain with horizontal length, $L_x \in [0, 2]$, and vertical length, $L_z \in [-1/2, 1/2]$, with no-slip, nonpenetrative top and bottom boundaries ($\mathbf{u} = [u, w] = 0$). All flows computed are periodic in the horizontal direction. Under the Boussinesq approximation the nondimensional equations describing the conservation of momentum, heat, and mass can be written as

$$\frac{1}{\text{Pr}}(\partial_t \mathbf{u} + \mathbf{u} \cdot \nabla \mathbf{u}) = -\nabla P + RT \mathbf{1}_z + \nabla^2 \mathbf{u}, \quad (5)$$

$$\partial_t T + \mathbf{u} \cdot \nabla T = \nabla^2 T, \quad (6)$$

$$\nabla \cdot \mathbf{u} = 0. \quad (7)$$

Here we have scaled length by the fluid layer depth, h , and time by the thermal diffusion time, h^2/κ . Pr is the Prandtl number [defined in Eq. (1)] and R is the thermal forcing parameter. The unit vector in the vertical is denoted $\mathbf{1}_z$. The form of R depends on the nature of the following thermal boundary conditions.

(i) The fixed-temperature cases have $T|_{z=\mp 1/2} = 1, 0$. Scaling temperature by the temperature difference across the layer, ΔT , gives the traditional Rayleigh number, $R = \text{Ra}$ [see Eq. (1)].

(ii) The fixed heat-flux cases have an imposed vertical flux ($\beta = -1$). Scaling length and time as before, and temperature by βh gives the flux Rayleigh number, Ra_F ,

$$R = \text{Ra}_F = \frac{\alpha g \beta h^4}{\nu \kappa}, \quad (8)$$

with boundary conditions $\partial_z T|_{\pm 1/2} = -1$.

Note that $\text{Ra}_F = \text{Ra Nu}$ and all results presented in this paper are shown in terms of Ra . For fixed heat-flux convection an increase in Ra and hence a better degree of mixing is achieved by the convection evolving to reduce the temperature difference between the top and bottom boundaries [42].

2. Rotating RBC

We have run a series of three-dimensional rotating convection simulations solving Eqs. (7) and (6) along with the momentum equation including the Coriolis term,

$$\frac{E}{\text{Pr}}(\partial_t \mathbf{u} + \mathbf{u} \cdot \nabla \mathbf{u}) + \mathbf{1}_z \times \mathbf{u} = -\nabla P + \text{RE}T \mathbf{1}_z + E \nabla^2 \mathbf{u}. \quad (9)$$

The extent in each horizontal direction is taken to be the same and the domain has horizontal lengths, $L_x = L_y \in [0, 2]$, and vertical length, $L_z \in [-1/2, 1/2]$. All flows computed are doubly periodic in the horizontal with top and bottom boundaries having free-slip boundary conditions on the velocity ($\mathbf{u} = [u, v, w]$):

$$\partial_z u|_{z=\pm 1/2} = 0, \quad \partial_z v|_{z=\pm 1/2} = 0, \quad w|_{z=\pm 1/2} = 0. \quad (10)$$

All rotating cases use fixed temperature boundary conditions and have $R = \text{Ra}$ [Eq. (1)].

B. Numerical implementation

The simulations use the open-source, pseudospectral code Dedalus ([43]; see [44] for more information). Spatial discretization is achieved using Fourier bases in the horizontal and Chebychev polynomial bases for the vertical direction. The spatial resolution for each simulation is described by the number of collocation points in each direction and is listed for all simulations in the Supplemental Material [45] with relevant numerical and physical parameters. Time stepping uses an implicit-explicit Runge Kutta method, with linear terms (diffusion, pressure, buoyancy, and Coriolis when present) treated implicitly and nonlinear terms treated explicitly.

All numerical simulations presented have $\text{Pr} = 1$. The temporal convergence of each numerical model is ensured by running for at least 100 advection time units (one advection time unit is the time taken for a fluid parcel to traverse the fluid layer, h/U). The simulations are in thermal and energetic equilibrium as indicated by satisfying the internal consistency checks for the Nusselt number and buoyant energy production [26,38,46] to within a 1% tolerance. Furthermore, the 1% residuals show that the simulations have adequate spatial resolution. The consistency checks only formally hold over an infinite time interval. We ensure temporal convergence in our simulations by comparing values of diagnostic quantities such as Nu over the entire averaging interval with the values corresponding to the first and second halves of this time interval. The percentage difference between these values is always within 5% and typically 2% for the vast majority of cases. The convergence criteria are summarized in the Supplemental Material. For the no-slip cases we compute the thickness of the mechanical boundary layers based on the local maxima of the horizontal velocity variations [26]. There are at least seven grid points in each mechanical boundary layer (most simulations have 10–15 points) and these resolutions are sufficient for resolving the structure of boundary layers in RBC [47,48].

The temporally averaged (denoted by an overbar) profile of temperature, T , averaged over horizontal surfaces (denoted by angled brackets) is denoted, ϑ ,

$$\vartheta = \overline{\langle T \rangle}, \quad (11)$$

where $\langle f \rangle = A^{-1} \int_A f dA$ with A corresponding to averaging in just x for two-dimensional cases and averaging in both x and y for three-dimensional cases. For all cases an exact measure of Nu is computed by evaluating the vertical derivative of the temperature on the boundaries:

$$\text{Nu} = -\partial_z \vartheta|_{\text{boundary}}. \quad (12)$$

This is an accurate definition owing to Chebychev differentiation.

C. Methods of defining δ

A number of different methods have been proposed to define the edge and hence the width of the TBL [15] and of these methods we describe the two most widely applied definitions: the linear intersection and local maxima methods. Following this we suggest a definition based on basic physical arguments informed by the heat equation termed the ‘‘heat transport’’ method.

1. Linear intersection method

The linear intersection method is derived from the shape of the ϑ profile [Fig. 1(a)] and a simple geometric argument is made to define δ . The linear (conductive) profile near the boundary is extrapolated to the linear gradient fit at middepth and this location defines δ [21–23]. For an isothermal bulk (as observed in nonrotating convection) this is equivalent to extrapolating the profile near the boundary to the isothermal value.

2. Local maxima method

The local maxima method assumes that the rms temperature fluctuations, σ ,

$$\sigma = \sqrt{\langle (T - \vartheta)^2 \rangle}, \quad (13)$$

have pronounced local maxima close to the boundaries. The location of this maxima corresponds to the location at which thermal plumes emitted from the TBL are mixed into the fluid bulk [24]. Consequently, this location also defines δ [26,49,50].

3. Heat transport method

We suggest an alternative definition of the TBL based on physical arguments on the conservation of heat. Boussinesq convection with no internal heat sources must conserve thermal energy, which can only be transferred via advection and conduction [Eq. (6)]. The dimensionless temperature conservation can be written in terms of the total heat-flux, \mathbf{q} :

$$\partial_t T = -\nabla \cdot \mathbf{q}, \quad \mathbf{q} = \underbrace{\mathbf{u}T}_{\text{advection}} - \underbrace{\nabla T}_{\text{conduction}}. \quad (14)$$

The vertical heat-flux is then given by

$$\mathbf{1}_z \cdot \mathbf{q} = wT - \partial_z T. \quad (15)$$

Within the TBL, conduction is dominant (advection is expected to be unimportant owing to the small vertical velocities near the nonpenetrative boundaries). For nonrotating convection, advective heat transport is dominant in the fluid bulk owing to the local temperature gradients being negligible. We suggest that a physically relevant definition for the TBL is given by the intersection of the two contributions in Eq. (14) [see Fig. 1(b)]; we refer to this as the ‘‘heat transport’’ method below.

III. RESULTS

We will systematically investigate the robustness of each of the three methods to define δ . First, we will consider the influence of the thermal boundary conditions on each method using simulations of nonrotating convection. Secondly, we investigate how each method performs when rotation is present. We test the methods through comparison with theoretical expectations and check self-consistency as well as consistency between different methods.

A. Influence of thermal boundary conditions

Equation (3) links δ with the global heat transport. To write this in terms of input parameters we use the Nu-Ra scaling behavior. Above $Ra = 10^6$ (and up to $Ra \leq 3 \times 10^8$) we find that the

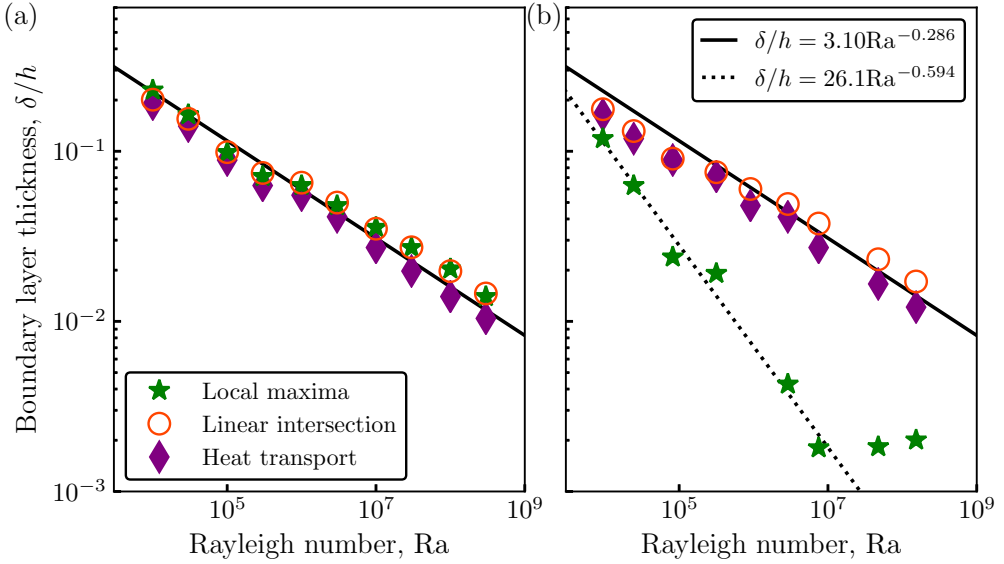


FIG. 2. Boundary layer thickness as a function of Rayleigh number for each of the different methods: (a) shows fixed temperature cases and (b) fixed heat-flux. The linear intersection (orange circles), local maxima (green stars), and heat transport (purple diamonds) methods are shown along with the scaling prediction shown as the dashed line. The scaling prediction of Eq. (16), $\delta/h \sim Ra^{-0.286}$, is shown as the solid line and the empirical fit $\delta/h \sim Ra^{-0.594}$ is shown for the fixed heat-flux case.

heat transfer data for both the fixed heat-flux and fixed temperature cases collapses onto a single scaling law,

$$Nu = 0.138 Ra^{0.286}. \quad (16)$$

This behavior is in good agreement with the $Nu \sim Ra^{2/7}$ behavior found for similar ranges of Ra [9,32,51]. It follows that the TBL thickness should scale as

$$\frac{\delta}{h} \sim Ra^{-2/7}. \quad (17)$$

Figure 2(a) shows that for fixed temperature boundaries all three methods are in good agreement with the theoretical prediction of Eq. (17). The empirical fits to the data with $Ra \geq 10^6$ give $\delta_{LI} = 2.52 Ra^{-0.26 \pm 0.02}$, $\delta_{LM} = 2.46 Ra^{-0.26 \pm 0.02}$, and $\delta_{HT} = 2.63 Ra^{-0.28 \pm 0.03}$ for the linear intersection, local maxima, and heat transport methods, respectively. All three fits have similar values of the mean relative misfit, χ (defined in [38,52]) in the range 1.4%–3.0%. In all cases the error in the empirically determined exponents arises from an unbiased estimator for the covariance of the data. Figure 2(b) shows that for fixed heat-flux boundaries the linear intersection and heat transport methods agree with the scaling prediction having empirical fits $\delta_{LI} = 2.47 Ra^{-0.26 \pm 0.02}$ and $\delta_{HT} = 3.31 Ra^{-0.28 \pm 0.04}$, respectively. The local maxima method gives a very different behavior when $Ra \geq 10^6$, $\delta_{LM} = 0.04 Ra^{-0.15}$, and a large misfit value, $\chi = 29.3\%$.

The linear intersection method works for either configuration because the temperature profile exhibits an isothermal fluid interior and two laminar thermal boundary layers which are insensitive to the choice of boundary conditions [see Figs. 1(a) and 3(a)]. Similarly, the heat transport definition is suitable for either boundary condition [Fig. 1(b) or 3(b)] and agrees well with the linear intersection prediction. In contrast, the local maxima method is suitable for boundaries with a prescribed fixed temperature as there is zero fluctuation on the boundary allowing well pronounced local maxima. In the fixed heat-flux case the fluctuations are free to evolve and the local maxima (when they do exist)

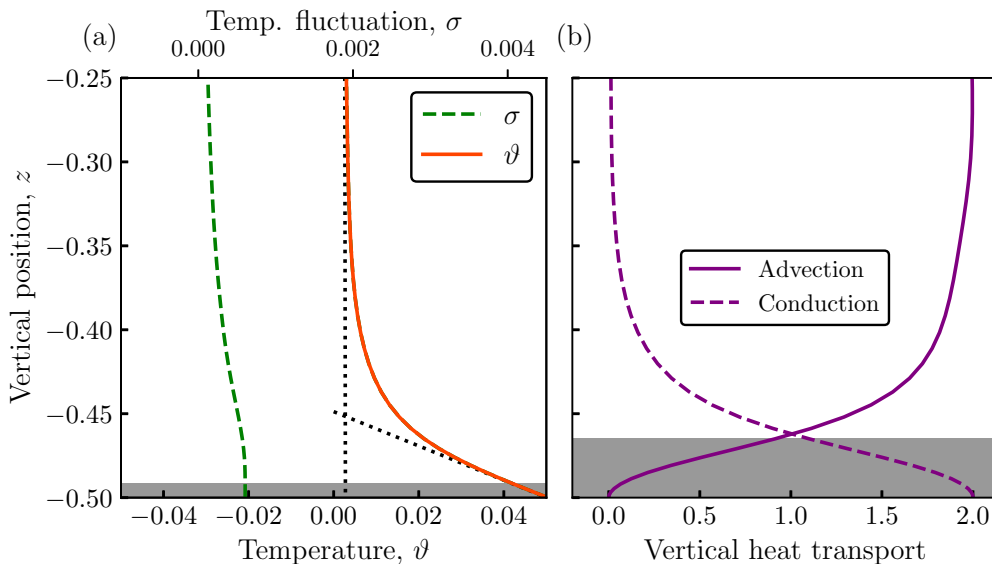


FIG. 3. Results from the model with $Ra = 2.89 \times 10^6$ and fixed heat-flux boundaries. Only the lowest quarter of the domain is shown to focus on behavior near the boundary. (a) Vertical profiles of temperature (solid orange) and rms fluctuation (dashed green). The dotted black lines show linear fits to ϑ at middepth and close to the boundaries. The gray shaded region shows the thermal boundary layer defined by the maxima in the σ profile. (b) Vertical profiles of advective (solid purple) and conductive (dashed purple) heat transport. The gray shaded regions show the intersection of the heat transport contributions.

are not well constrained [see Fig. 3(a)]. For the cases where a TBL can be identified, it can be as much as an order of magnitude smaller than the other definitions. The TBL thickness determined by the local maxima method scales as $\delta_{LM} \sim Ra^{-0.59}$ for $Ra \leq 10^7$, which is steeper than any behavior that we know of. The most extreme cases plateau off due to the value being bounded by numerical resolution.

B. Effects of rotation

Unlike nonrotating convection there is no well established scaling behavior for the heat transfer in rotating systems with no-slip boundaries. The heat transfer scales as $Nu \sim Ra^{\lambda(E)}$ and λ increases monotonically with decreasing E [9,29] due to larger Ekman pumping effects [39]. Consequently, there is no prediction for the scaling behavior of δ which holds over all $Ra - E$ parameter space.

In rapidly rotating convection a significant fraction of the temperature difference is accommodated in the fluid bulk [Fig. 4(a)]. There is no current consensus on how the magnitude of these internal temperature gradients depends on the input parameters [15,26]. If we assume that the bulk rather than the boundary layers (as in nonrotating convection) controls the heat transport and assume viscous dissipation is negligible in the interior, Nu becomes independent of diffusive effects and follows the scaling [11,53]

$$Nu \sim Ra^{3/2} E^2 Pr^{-1/2}. \quad (18)$$

This heat transfer behavior has been observed in rapidly rotating convection (low E) when free-slip boundaries are used [10]. An alternative expression for the ratio of total heat transport to conductive heat transport is given by

$$Nu = \frac{\delta \vartheta}{\Delta \vartheta} \frac{h}{\delta}, \quad (19)$$

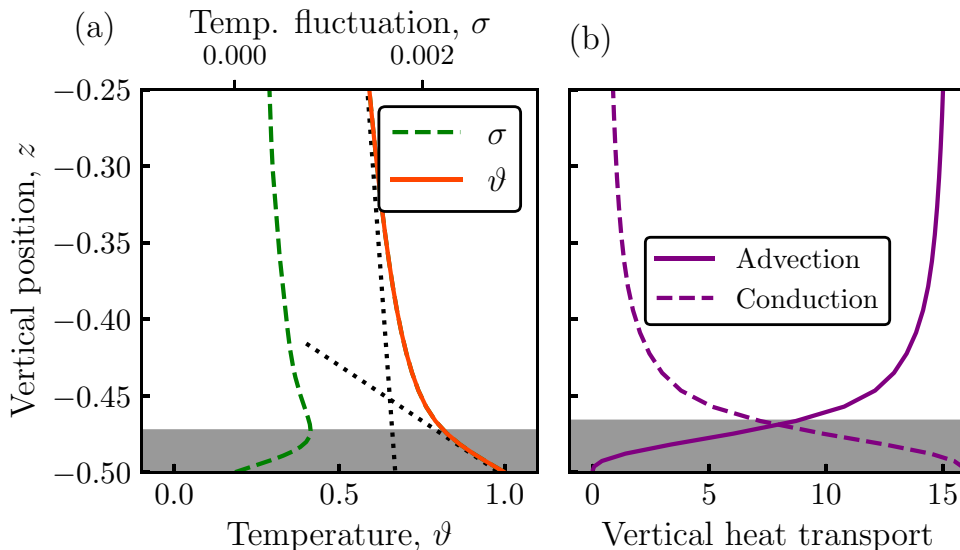


FIG. 4. Results from the model with $Ra = 5 \times 10^{11}$, $E = 10^{-7}$, and fixed temperature boundaries. Only the lowest quarter of the domain is shown to focus on behavior near the boundary. (a) Vertical profiles of temperature (solid orange) and rms fluctuation (dashed green). The dotted black lines show linear fits to ϑ at middepth and close to the boundaries. The gray shaded region shows the thermal boundary layer defined by the maxima in the σ profile. (b) Vertical profiles of advective (solid purple) and conductive (dashed purple) heat transport. The gray shaded regions show the intersection of the heat transport contributions.

where $\delta\vartheta$ is the temperature drop across the TBL. This expression is obtained by assuming that, over the thickness, δ , the temperature profile is linear and we estimate conductive heat transport near the boundary as $\partial_z T \sim \delta\vartheta/\delta$ and nondimensionalize appropriately. Equation (19) provides a consistency check for each of the three methods proposed to define δ by comparing the exact value of Nu [given by Eq. (12)] with the prediction of Eq. (19) from the values of δ/h and $\delta\vartheta/\Delta\vartheta$ obtained from the simulations. An appropriate definition of the boundary layer should consistently predict the actual temperature gradient across the boundary [Eq. (12)] with an estimate based on the system scale [Eq. (19)].

Figure 5(a) shows that our suite of rotating convection simulations with $E = 10^{-7}$ conform to the diffusion-free scaling behavior [Eq. (18)]. In Fig. 5(b) we show the relative error in the predictions of Nu for each method of defining δ . The local maxima and heat transport methods give excellent agreement with Nu and their predictions typically have an error of approximately 1%. The linear intersection method predicts Nu with an error of 3%–6%. The error in the predictions of Nu [using Eq. (19)] can be interpreted by investigating the scaling behavior of δ and $\delta\vartheta$. For rotating convection we find that the TBL thickness predicted by the local maxima and heat transport methods scales as $\delta_{HT} \sim Ra^{-1.9 \pm 0.04}$ (Fig. 6) with the temperature drop across the boundary layer, $\delta\vartheta \sim Ra^{-0.56 \pm 0.05}$. These methods accurately recover the Nu - Ra scaling in Eq. (18) and the two scaling laws are in agreement with models derived in the limit of asymptotically small E [15]. The linear intersection is distinguishably different with $\delta_{LI} \sim Ra^{-1.5 \pm 0.03}$ [Fig. 6(a)] and $\delta\vartheta \sim Ra^{-0.09 \pm 0.01}$ [Fig. 6(b)]. The linear intersection method predicts thicker boundary layers than the other methods in the fully nonlinear regime and has a lower scaling exponent for the Ra dependence of both δ/h and $\delta\vartheta/\Delta\vartheta$. This leads to the linear intersection method predicting $Nu \sim Ra^{1.41}$ giving a larger error when compared with the observed scaling $Nu \sim Ra^{3/2}$. We note that our data covers only a single decade in Ra and it is difficult to distinguish between the empirical scaling laws which have quite similar exponents; however, if Nu is estimated by δ defined using the linear intersection method Nu is off by $\approx 5\%$.

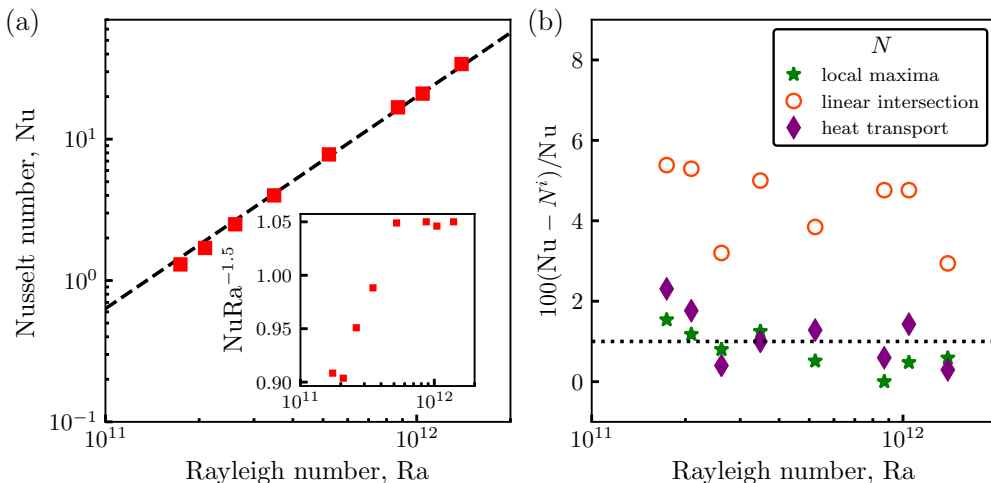


FIG. 5. (a) Nusselt number versus Rayleigh number for convection between free-slip boundaries with $E = 10^{-7}$. The diffusive-free scaling [Eq. (18)] is shown as the dashed line. (b) Percentage error in the Nusselt number prediction of Eq. (19) for each of the three methods, N^i , with the value of Eq. (12), Nu . The dotted line corresponds to an error of 1%.

IV. DISCUSSION

We have investigated two commonly used methods for defining the thermal boundary layer using simulations of Rayleigh-Bénard convection with and without rotation. We have shown that the local maxima method works well for specific configurations, whereas the linear intersection method can be applied more generally. The location of the maxima in the rms temperature fluctuation succeeds in predicting the thermal boundary layer thickness for fixed temperature convection but fails when the boundaries are prescribed a fixed heat-flux. In the fixed heat-flux case the temperature fluctuation on the boundary is nonzero and the local maxima that develop are not well pronounced. This

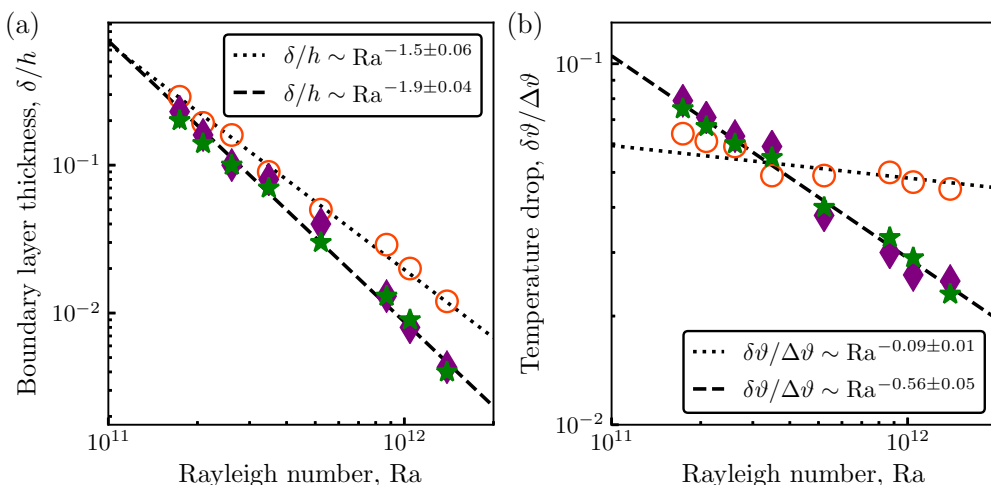


FIG. 6. Boundary layer thickness (a) and temperature drop across the boundary layer (b) versus Rayleigh number for simulations with $E = 10^{-7}$. The linear intersection (orange circles), local maxima (green stars), and heat transport (purple diamonds) methods are shown along with the empirical fits shown as dashed and dotted lines. The local maxima and heat transport scalings are indistinguishable in this case and therefore jointly fit.

helps explain the observation of Verzicco and Sreenivasan [33] who found that the local maxima method predicted a boundary layer of zero thickness when the boundary was prescribed a fixed heat-flux. The intersection of linear fits near the boundary and in the interior is applicable to well mixed systems but is less intuitively applied when interior gradients are present (typically seen in rotationally constrained convection). When defined using the linear intersection method, the thermal boundary layer thickness and the associated temperature drop across the boundary layer are less adequate in predicting the Nusselt number. Clearly, both established methods are limited and we show that the most robust treatment of the thermal boundary layer thickness is achieved by locating the crossover in advective and conductive contributions to the heat transport. This heat transport method can be applied to either fixed temperature or fixed heat-flux thermal boundary conditions in both rotating and nonrotating systems.

The nonrotating simulations presented in this paper are two-dimensional with a fixed aspect ratio, $\Gamma = 2$, and Prandtl number, $Pr = 1$. The comparative study of Schmalzl *et al.* [54] showed that for $Pr \geq 1$ there is good agreement between two- and three-dimensional convection simulations; in particular, the temperature profiles are almost indistinguishable. We tested the effect of different aspect ratios by running a set of simulations with $Pr = 1$ and $Ra = 10^7$ and $\Gamma \in \{2, 4, 8, 16\}$. The heat transport method is insensitive to changing Γ with the two heat transport contributions having a clear crossover in all cases. Next, we have run a suite of simulations with $\Gamma = 2$, and $Ra = 10^7$ with varying Prandtl number, $\log_{10}(Pr) \in \{0, 1, 2\}$. The heat transport method can be applied regardless of Pr , whereas for high Pr ($Pr = 100$) the linear intersection method becomes difficult to implement due to an overshoot in the temperature profile of its mean value [55,56]. Our analysis of each method to define the TBL can be broadly applied to convection simulations for any aspect ratio, Rayleigh number, and Prandtl number of unity or above.

In contrast to numerical simulations, laboratory convection does not have access to the same wealth of diagnostic capabilities. Experimental studies of a single plume have measured velocity and temperature simultaneously with sufficient resolution to locate the crossover in vertical heat transport [57,58]. Rotating convection experiments are now able to measure heat-transfer and flow speed data simultaneously [59] and so the heat transport method can be applied in a laboratory setting.

The heat transport method could prove useful for identifying boundary layers for any scalar field governed by an advection-diffusion equation; e.g., the boundary layer in compositional convection [60].

ACKNOWLEDGMENTS

R.S.L. is supported by the Engineering and Physical Sciences Research Council (EPSRC) Centre for Doctoral Training in Fluid Dynamics (Grant No. EP/L01615X/1). C.J.D. is supported by a Natural Environment Research Council (NERC) Independent Research Fellowship (No. NE/L011328/1). S.M.T. would like to acknowledge support from the European Research Council (ERC) under the European Union's Horizon 2020 research and innovation program (Agreement No. D5S-DLV-786780). We would like to thank C. Lithgow-Bertelloni and J. Aurnou (both UCLA) for useful discussions. We would like to thank two anonymous reviewers for suggestions that improved this manuscript. This work used ARC2 and ARC3, part of the High Performance Computing facilities at the University of Leeds. Figures were produced using Matplotlib [61].

The authors report no conflict of interest.

[1] A. D. Brent, V. R. Voller, and K. T. J. Reid, Enthalpy-porosity technique for modeling convection-diffusion phase change: Application to the melting of a pure metal, *Numer. Heat Transfer, Part A* **13**, 297 (1988).

- [2] M. Heimpel, J. Aurnou, and J. Wicht, Simulation of equatorial and high-latitude jets on Jupiter in a deep convection model, *Nature (London)* **438**, 193 (2005).
- [3] M. S. Miesch, The coupling of solar convection and rotation (invited review), in *Helioseismic Diagnostics of Solar Convection and Activity* (Springer, Berlin, 2000), pp. 59–89.
- [4] S. I. Braginsky and P. H. Roberts, Equations governing convection in Earth’s core and the geodynamo, *Geophys. Astrophys. Fluid Dyn.* **79**, 1 (1995).
- [5] F. Busse, Convective flows in rapidly rotating spheres and their dynamo action, *Phys. Fluids* **14**, 1301 (2002).
- [6] H. Rossby, A study of Bénard convection with and without rotation, *J. Fluid Mech.* **36**, 309 (1969).
- [7] D. Funfschilling, E. Brown, A. Nikolaenko, and G. Ahlers, Heat transport by turbulent Rayleigh–Bénard convection in cylindrical samples with aspect ratio one and larger, *J. Fluid Mech.* **536**, 145 (2005).
- [8] J. Aurnou, Planetary core dynamics and convective heat transfer scaling, *Geophys. Astrophys. Fluid Dyn.* **101**, 327 (2007).
- [9] E. M. King, S. Stellmach, J. Noir, U. Hansen, and J. M. Aurnou, Boundary layer control of rotating convection systems, *Nature (London)* **457**, 301 (2009).
- [10] S. Stellmach, M. Lischper, K. Julien, G. Vasil, J. S. Cheng, A. Ribeiro, E. M. King, and J. M. Aurnou, Approaching the Asymptotic Regime of Rapidly Rotating Convection: Boundary Layers Versus Interior Dynamics, *Phys. Rev. Lett.* **113**, 254501 (2014).
- [11] K. Julien, E. Knobloch, A. M. Rubio, and G. M. Vasil, Heat Transport in Low Rossby Number Rayleigh–Bénard Convection, *Phys. Rev. Lett.* **109**, 254503 (2012).
- [12] S. Grossmann and D. Lohse, Scaling in thermal convection: A unifying theory, *J. Fluid Mech.* **407**, 27 (2000).
- [13] S. Grossmann and D. Lohse, Prandtl and Rayleigh number dependence of the Reynolds number in turbulent thermal convection, *Phys. Rev. E* **66**, 016305 (2002).
- [14] S. Grossmann and D. Lohse, Multiple scaling in the ultimate regime of thermal convection, *Phys. Fluids* **23**, 045108 (2011).
- [15] K. Julien, A. Rubio, I. Grooms, and E. Knobloch, Statistical and physical balances in low Rossby number Rayleigh–Bénard convection, *Geophys. Astrophys. Fluid Dyn.* **106**, 392 (2012).
- [16] E. Bodenschatz, W. Pesch, and G. Ahlers, Recent developments in Rayleigh–Bénard convection, *Annu. Rev. Fluid Mech.* **32**, 709 (2000).
- [17] M. Plumley and K. Julien, Scaling laws in Rayleigh–Benard convection, *Earth Space Sci.* **6**, 1580 (2019).
- [18] W. V. R. Malkus, The heat transport and spectrum of thermal turbulence, *Proc. R. Soc. London A* **225**, 196 (1954).
- [19] E. A. Spiegel, Convection in stars I. Basic Boussinesq convection, *Annu. Rev. Astron. Astrophys.* **9**, 323 (1971).
- [20] A. Belmonte, A. Tilgner, and A. Libchaber, Temperature and velocity boundary layers in turbulent convection, *Phys. Rev. E* **50**, 269 (1994).
- [21] R. Verzicco and R. Camussi, Prandtl number effects in convective turbulence, *J. Fluid Mech.* **383**, 55 (1999).
- [22] M. Breuer, S. Wessling, J. Schmalzl, and U. Hansen, Effect of inertia in Rayleigh–Bénard convection, *Phys. Rev. E* **69**, 026302 (2004).
- [23] Y. Liu and R. E. Ecke, Local temperature measurements in turbulent rotating Rayleigh–Bénard convection, *Phys. Rev. E* **84**, 016311 (2011).
- [24] A. Tilgner, A. Belmonte, and A. Libchaber, Temperature and velocity profiles of turbulent convection in water, *Phys. Rev. E* **47**, R2253 (1993).
- [25] E. King, S. Stellmach, and J. Aurnou, Heat transfer by rapidly rotating Rayleigh–Bénard convection, *J. Fluid Mech.* **691**, 568 (2012).
- [26] E. King, S. Stellmach, and B. Buffett, Scaling behaviour in Rayleigh–Bénard convection with and without rotation, *J. Fluid Mech.* **717**, 449 (2013).
- [27] Y. B. Xin and K. Q. Xia, Boundary layer length scales in convective turbulence, *Phys. Rev. E* **56**, 3010 (1997).

- [28] R. Du Puits, C. Resagk, A. Tilgner, F. Busse, and A. Thess, Structure of thermal boundary layers in turbulent Rayleigh–Bénard convection, *J. Fluid Mech.* **572**, 231 (2007).
- [29] J. Cheng, S. Stellmach, A. Ribeiro, A. Grannan, E. King, and J. Aurnou, Laboratory-numerical models of rapidly rotating convection in planetary cores, *Geophys. J. Intl.* **201**, 1 (2015).
- [30] D. Hurler, E. Jakeman, and E. R. Pike, On the solution of the Bénard problem with boundaries of finite conductivity, *Proc. R. Soc. London A* **296**, 469 (1967).
- [31] J. Von Hardenberg, A. Parodi, G. Passoni, A. Provenzale, and E. Spiegel, Large-scale patterns in Rayleigh–Bénard convection, *Phys. Lett. A* **372**, 2223 (2008).
- [32] H. Johnston and C. R. Doering, Comparison of Turbulent Thermal Convection between Conditions of Constant Temperature and Constant Flux, *Phys. Rev. Lett.* **102**, 064501 (2009).
- [33] R. Verzicco and K. Sreenivasan, A comparison of turbulent thermal convection between conditions of constant temperature and constant heat flux, *J. Fluid Mech.* **595**, 203 (2008).
- [34] C. A. Jones, Planetary magnetic fields and fluid dynamos, *Annu. Rev. Fluid Mech.* **43**, 583 (2011).
- [35] J. Aurnou, M. Calkins, J. Cheng, K. Julien, E. King, D. Nieves, K. Soderlund, and S. Stellmach, Rotating convective turbulence in earth and planetary cores, *Phys. Earth Planet. Inter.* **246**, 52 (2015).
- [36] S. Schmitz and A. Tilgner, Heat transport in rotating convection without Ekman layers, *Phys. Rev. E* **80**, 015305(R) (2009).
- [37] T. Gastine, J. Wicht, and J. Aubert, Scaling regimes in spherical shell rotating convection, *J. Fluid Mech.* **808**, 690 (2016).
- [38] R. Long, J. Mound, C. Davies, and S. Tobias, Scaling behaviour in spherical shell rotating convection with fixed-flux thermal boundary conditions, *J. Fluid Mech.* **889**, A7 (2020).
- [39] H. P. G. Greenspan, *The Theory of Rotating Fluids* (CUP Archive, Cambridge, UK, 1968).
- [40] J. Pedlosky, *Geophysical Fluid Dynamics* (Springer Science & Business Media, New York, 2013).
- [41] K. Julien, S. Legg, J. McWilliams, and J. Werne, Rapidly rotating turbulent Rayleigh–Bénard convection, *J. Fluid Mech.* **322**, 243 (1996).
- [42] D. Goluskin, *Internally Heated Convection and Rayleigh–Bénard Convection* (Springer, New York, 2016).
- [43] K. J. Burns, G. M. Vasil, J. S. Oishi, D. Lecoanet, and B. Brown, Dedalus: Flexible framework for spectrally solving differential equations, Astrophysics Source Code Library, 2016.
- [44] <http://dedalus-project.org/>.
- [45] See Supplementary Material at <http://link.aps.org/supplemental/10.1103/PhysRevFluids.5.113502> for numerical details and additional media.
- [46] J. E. Mound and C. J. Davies, Heat transfer in rapidly rotating convection with heterogeneous thermal boundary conditions, *J. Fluid Mech.* **828**, 601 (2017).
- [47] R. Verzicco and R. Camussi, Numerical experiments on strongly turbulent thermal convection in a slender cylindrical cell, *J. Fluid Mech.* **477**, 19 (2003).
- [48] R. J. Stevens, R. Verzicco, and D. Lohse, Radial boundary layer structure and Nusselt number in Rayleigh–Bénard convection, *J. Fluid Mech.* **643**, 495 (2010).
- [49] A. Tilgner, High Rayleigh number convection in spherical shells, *Phys. Rev. E* **53**, 4847 (1996).
- [50] R. P. Kunnen, R. Ostilla-Mónico, E. P. Van Der Poel, R. Verzicco, and D. Lohse, Transition to geostrophic convection: the role of the boundary conditions, *J. Fluid Mech.* **799**, 413 (2016).
- [51] A. Clarke, C. Davies, D. Ruprecht, S. Tobias, and J. S. Oishi, Performance of parallel-in-time integration for Rayleigh–Bénard convection, *Comput. Visual Sci.* **23**, 10 (2020).
- [52] U. R. Christensen and J. Aubert, Scaling properties of convection-driven dynamos in rotating spherical shells and application to planetary magnetic fields, *Geophys. J. Intl.* **166**, 97 (2006).
- [53] C. A. Jones, Thermal and compositional convection in the outer core, in *Treatise on Geophysics*, 2nd ed., edited by G. Schubert (Elsevier, Amsterdam, 2015), Vol. 8, pp. 115–159.
- [54] J. Schmalzl, M. Breuer, and U. Hansen, On the validity of two-dimensional numerical approaches to time-dependent thermal convection, *Europhys. Lett.* **67**, 390 (2004).
- [55] U. Hansen, D. A. Yuen, and A. V. Malevsky, Comparison of steady-state and strongly chaotic thermal convection at high Rayleigh number, *Phys. Rev. A* **46**, 4742 (1992).
- [56] J. Schmalzl, M. Breuer, and U. Hansen, The influence of the Prandtl number on the style of vigorous thermal convection, *Geophys. Astrophys. Fluid Dyn.* **96**, 381 (2002).

- [57] N. Cagney, W. H. Newsome, C. Lithgow-Bertelloni, A. Cotel, S. R. Hart, and J. A. Whitehead, Temperature and velocity measurements of a rising thermal plume, [Geochem. Geophys. Geosyst.](#) **16**, 579 (2015).
- [58] N. Cagney and C. Lithgow-Bertelloni, Dynamics and excess temperature of a plume throughout its life cycle, [Geophys. J. Intl.](#) **205**, 1574 (2016).
- [59] E. K. Hawkins, J. S. Cheng, T. Pilegard, S. Stellmach, K. Julien, and J. M. Aurnou, Observing geostrophic turbulence in laboratory models of planetary core convection, [Geophys. J. Intl.](#) (to be published) (2020).
- [60] M. Bouffard, S. Labrosse, G. Choblet, A. Fournier, J. Aubert, and P. J. Tackley, A particle-in-cell method for studying double-diffusive convection in the liquid layers of planetary interiors, [J. Comput. Phys.](#) **346**, 552 (2017).
- [61] J. D. Hunter, Matplotlib: A 2D graphics environment, [Comput. Sci. Eng.](#) **9**, 90 (2007).